Image Enhancement using Calibrated Lens Simulations

Yichang Shih[1,2], Brian Guenter[1], Neel Joshi[1]

Microsoft Research[1], MIT CSAIL[2]

Abstract. All lenses have optical aberrations which reduce image sharpness. These aberrations can be reduced by deconvolving an image using the lens point spread function (PSF). However, fully measuring a PSF is laborious and prohibitive. Alternatively, one can simulate the PSF if the lens model is known. However, due to manufacturing tolerances lenses differ subtly from their models, so often a simulated PSF is a poor match to measured data. We present an algorithm that uses a PSF measurement at a single depth to calibrate the nominal lens model to the measured PSF. The calibrated model can then be used to compute the PSF for any desired setting of lens parameters for any scene depth, without additional measurements or calibration. The calibrated model gives deconvolution results comparable to measurement but is much more compact and require hundreds of times fewer calibration images.

1 Introduction

Lens aberrations limit the quality of images formed by lenses. These aberrations are inherent in the physics of optical image formation and vary as a function of lens settings. Image deconvolution can be used to reduce many aberrations if the lens point spread function (PSF) is known. Recovering both the PSF and deblurred image from a single image input (blind-deconvolution) is ill-posed and as a result can be unreliable.

An alternative is to measure the PSF of a lens. Indirect method such as that of Joshi et al. [11] over-smooth the PSF unacceptably as a result of regularization needed in their method. Direct methods include using a laser, beam spreader, and precision collimator system to create a single illumination point for measuring the PSF one point at a time. These methods require precise hardware and are very slow. The more commonly used, faster method is to capture an image of a grid of back illuminated pinholes, such as shown in Fig. 5. Each photograph captures many samples of the PSF across the entire field of view. The complete PSF can be measured by systematically varying the lens parameters to cover all possible permutations.

Unfortunately, making a pinhole target small enough so that they image less than a pixel is very difficult, especially for close focusing distance. [1]. Not being able to measure near the lens [2], where the PSF varies most rapidly, is a significant limitation to direct measurement of PSFs.

An equally serious problem is the sheer number of photographs necessary to adequately sample the PSF. Simulations with the commercial Zemax lens design software has shown that lens PSF varies substantially as a function of lens parameters, including

---

[1] e.g. for a 2 micron pixel sensor to measure closer than 10 times the focal length of a lens, ones needs pinholes less than 20 microns in diameter. This is difficult both due to due to manufacturing limits and that diffraction through the pinhole becomes a factor

[2] typically on the order of a few feet for common focal length and sensor sizes
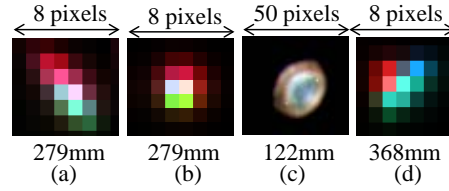
Fig. 1: Measured PSFs show that real lenses violate many common assumptions about the invariance of the PSF. The PSF is measured at (a) corner of a focused plane at 279mm, (b) center of the same focused plane, (c) corner of a de-focused plane (focusing at 279mm but imaged at 122mm), and (d) corner of a focused plane at 368mm.

aperture, focal length, focusing distance, and illuminant spectrum. The latter two parameters have generally been ignored in previous work in this area but they affect the PSF as strongly as the first two. As a result, literally hundreds of images are needed to properly measure the multidimensional parameter space of a lens. [3]

In addition, because the focusing distance and illuminant spectrum dimensions are difficult to sample along their full range, extrapolation beyond the captured data values will almost certainly be necessary. While interpolation is potentially possible, extrapolation is unlikely to work well, given the complex changes in the shape and amplitude of the PSF as a function of these two parameters.

An alternative is to simulate the lens PSF for any desired setting of lens parameters by using optics simulation on an accurate CAD model of the lens. The CAD model is called the lens prescription. The primary difficulty with using the lens prescription directly is that manufacturing tolerances [17] cause any particular physical lens to differ from the nominal CAD lens design, which causes dramatic PSF variations between nominally identical lenses, as shown in Fig. 4. As a consequence simply using the nominal lens prescription to generate PSF's for deconvolution doesn't give very good results.

---

[3] An accurate PSF measurement would require at least an additional 5 samples in the focusing distance dimension (aperture, focal length, focusing distance). At least another 3 samples would be necessary along the spectral dimension. A very conservative estimate of the total number of pictures required to accurately measure a lens PSF is $3 * 5^3 = 375$. In practice far more would be necessary for fast lenses that focus at close distances.
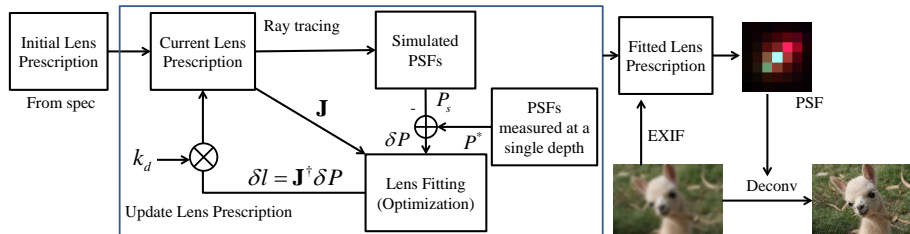

Fig. 2: Algorithm and system overview. Our lens prescription calibration process is illustrated in the blue outline. The process takes measured PSFs at a single depth as input. The process only need to be done once. We compute PSFs using calibrated lens prescription and EXIF info from the new input photo (focusing distance, aperture size, and white balance as approximate illuminant spectrum) for image enhancement.

Our approach is to use the lens prescription as a starting point for calibration process that adjusts the lens prescription to fit a single measurement of the PSF. The lens prescription fitting is done only once per lens. Once we have the lens prescription we can compute the PSF at any point on the image plane, for any combination of lens parameters: aperture, focal length, focusing distance, and illuminant. The technique overview is illustrated in Fig. 2.

This method has many advantages over direct PSF measurement because it requires far fewer calibration pictures (one versus hundreds), the fitted lens prescription is more compact than a full set of measured PSF images (a few hundred bytes versus hundreds of KBytes), and the PSF can be computed for arbitrary lens parameters, while measured PSF's only cover the range of lens parameters that were sampled and cannot be effectively extrapolated beyond this range.

For consumer level cameras lens manufacturers can use our method to calibrate each lens before it leaves the factory. For computer vision research applications lens prescriptions are frequently available for machine vision style lenses [4] so researchers can use the method to calibrate their systems.

The key contribution of this paper is the use of optics simulation combined with the fitting algorithm, which makes it possible to use a single calibration photograph to generate synthetic PSF's for any combination of lens settings.

2   Related Work

Much of the recent work in image deblurring has been in measuring and removing blur due to camera motion [7, 21] or scene motion [15, 16], while less attention has been paid towards correcting for blur due to lens aberrations, which is the situation we consider in this work.

Aberrations can be removed by deconvolving with the lens PSF [20]. Because of the high dimensionality of the PSF function and the difficulty of PSF measurement, corrections are usually performed by fitting the PSFs to a parametric model [13, 4, 2].

The closest related works are those of single image calibration and measurement methods [11, 3, 12]. These works show how to estimate optical blur functions or chromatic abberation either blindly or through a calibration process.

Simple spatially invariant parametric models are not accurate measures of image blur [11, 13]. Perhaps the most closely related works are those that have used or created lens models for image correction [6, 10, 9, 5, 14, 13]. Several commercial products, such as PTLens, DXO, and Adobe Photoshop, perform image corrections using non-physical low order parametric models tuned to various lens profiles. Due to their non-physical nature, these methods can only produce limited improvements [13].

Kee et al. [13] address this issue by presenting a spatially-varying parametric model fitted from estimated PSFs. Instead of estimating PSF from edge response in their work, we directly measure PSFs to avoid over-blurred PSFs [11]. We fits a lens CAD model so that we can predict PSFs at arbitrary aperture, focal length, focusing distance, illuminant spectrum. The latter two are ignored in Kee et al.'s work. Our method only requires a single photograph, which makes the calibration process far less laborious.

[4] Edmund Optics makes lens prescriptions available for research purposes. All our lenses were purchased there.

3   PSF simulation

Several previous works have made simplifying assumptions about the lens point spread function [4, 2, 19]. These simplifications include: 1) a simple canonical PSF shape, such as a 2D Gaussian, or pillbox, 2) a constant PSF across the image plane, 3) that the PSF is invariant as a function of distance to the focused object plane, and 4) that the defocused PSF is a scaled version of the focused PSF.

Real lenses violate all these assumptions. In Fig. 1, we show the measured PSF of a lens at two image positions, two focus/defocus distances, and two focal plane depths. Even on the optical axis, there are significant differences between the PSF; off-axis the differences are dramatic. Perhaps most surprisingly, the PSF is strongly dependent on the distance the lens is focused.

In the general case, the PSF of a fixed focal length lens is a 6 dimensional function of the light wavelength, (λ), image plane coordinates, (x, y), lens aperture, a, lens to object distance, d_{obj}, and back focal distance, d_{bf}. One can measure PSFs for a particular lens by taking measurements of the lens response over these 6 dimensions, using specialized equipment [22], but such methods are only accurate in limited working volumes and require a vast amount of data to be collected.

Modern lenses are designed using lens CAD models and are precisely specified by a set of parametric values called the *lens prescription*. Our method takes a single photograph to calibrate the lens prescription. The fitted lens model is used to generate PSFs at any desired lens parameter values. Given this specification, obtaining accurate PSFs becomes a software process instead of a complicated measurement process.

3.1   Lens Prescriptions

The lens prescription describes the optical properties of the lens: the size, curvature, index of refraction, and type of coating of each element. To account for chromatic aberration, a dispersion function models the variation of the index of refraction, n, with light wavelength, λ. The most commonly used functions are polynomials in either the Schott

$$n^2 = a_0 + a_1\lambda^2 + a_2\lambda^{-22} + a_3\lambda^{-4} + a_4\lambda^{-6} + a_5\lambda^{-8} \qquad (1)$$

or the Sellmeier 1 form

$$n^2 - 1 = \frac{K_1\lambda^2}{\lambda^2 - L_1} + \frac{K_2\lambda^2}{\lambda^2 - L_2} + \frac{K_3\lambda^2}{\lambda^2 - L_3}. \qquad (2)$$

We model the effect of the following parameters: 1) geometric properties of each optical surface: diameter, radius of curvature, offset along optical axis, and offset perpendicular to optical axis, 2) coefficients of the dispersion function of each material, 3) index of refraction and thickness of each antireflection coating material, and 4) lens back focal distance.

Our simulator currently models lens elements with spherical surfaces[5] and a single layer antireflection coating. We simulated three lenses from the Edmund Optics catalog [6]: a high resolution 6mm microvideo lens, a medium resolution 12mm microvideo lens,

---

[5] Aspherical surfaces are used in very high quality (and cost) glass lenses and in low cost plastic injection molded lenses. The majority of lenses between these extremes use only spherical surfaces.

[6] Chosen because they are typical machine vision lenses, and because Edmund Optics provides lens prescriptions for research purposes.

6mm #58202

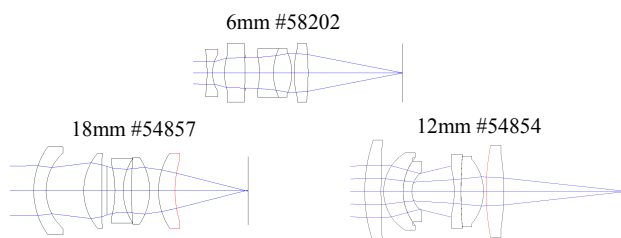18mm #54857   12mm #54854

Fig. 3: The 3 lenses we tested. All three lenses are stock Edmund Optics lenses – the part numbers are shown.

and a high resolution 18mm double Gauss lens. The optical layouts of all three shown in Fig. 3.

3.2   PSFs Computation with a Lens Prescription

Existing commercial software products, such as ZEMAX, can be used to simulate lenses, but as these products are costly and not instrumented to be used easily for an optimization or calibration procedure. Thus we have implement at standard lens simulator algorithm that uses the same principles as Zemax [8].

Given the focal length, aperture, focusing distance, and white balance that is stored in the EXIF header of the image file, we can simulate the image plane PSF of each of the virtual object points. We note that we do not need the full scene depth only the focal depth, since we only seek to remove aberrations and focal plane artifacts as opposed to defocus debluring – there are no limitations on the scene depth range. These PSF's are fed into the deconvolution algorithm to correct lens aberrations. In the interest of space, and as the contribution of our work is the calibration process and not the simulation, we describe the simulation details in our supplementary materials.

Because the PSF is dependent on wavelength we simulate the PSF at 18 wavelengths for each color channel and sum these incoherently to give the final PSF for each color channel. Our measurements are done with sequential RGB illumination from a three color LED lamp, so that artifacts due to demosaicing would not be confounded with the results of the image corrections; however, our methods can be easily be used with Bayer demosaicked images.

We assume most sensor has a microlens array as an anti-aliasing filter to create a 100% fill-factor. We thus model our sensor response linear to light intensity. We do not directly consider other effects. More in-depth study is a good suggestion for future work.

3.3   Mismatch with Measured PSFs

We measured actual lens PSFs and compared them with the simulated PSFs, as shown in Fig. 4. The measurement setup and method are described in Sec. 5. Note that the simulated PSFs are very different from measured PSFs. The mismatch is caused by variations within manufacturing tolerances and fabrication errors during lens production. Variation between nominally identical lenses can be quite large and also different from the lens specification [17].

Measured PSFs

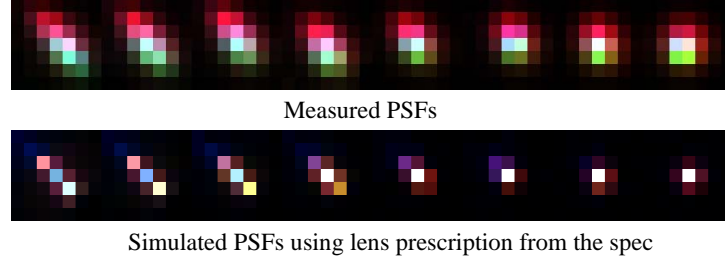Simulated PSFs using lens prescription from the spec

Fig. 4: Mismatch between a measured PSF and one simulated using the nominal, manufacturer provided lens prescription. Left to right in the two figures corresponds to the PSF being sampled from corner to center.

4   Lens Prescription Calibration

We notate our simulation by using the function $S(l, x)$, which takes a lens prescription l and light source positions x as input, and outputs the corresponding point spread functions P. Let l^* and l_s denote the actual and nominal lens specification, respectively. The object of the lens fitting step is to find $\delta l^* \equiv l^* - l_s$.

Our optimization method minimizes the L2 norm between the measured and the simulated PSFs by adjusting the lens prescription. Denoting the measured PSFs as P^*, the objective function is

$$\delta l^* = \arg\min_{\delta l} \| S(l_s + \delta l, x) - P^* \|_2. \tag{3}$$

Given that δl is very small and S is smooth around l_s, the first order approximation on $S(l_s + \delta l, x)$ is

$$S(l_s + \delta l, x) \approx S(l_s) + \frac{\partial S}{\partial l} \delta l, \tag{4}$$

where $S(l_s)$ is the PSF simulated using the nominal lens prescription, and $\frac{\partial S}{\partial l}$ is the Jacobian at l_s, which is denoted by $\mathbf{J}$. In practice, since there is no simple analytical form of $S(l_s)$, we perturb lens prescription and compute the PSF difference over the lens prescription variation to form the Jacobian matrix. Denoting $\delta P = P^* - S(l_s)$ as the difference between simulated and measured PSFs and combining Eq. 3 and Eq. 4 gives

$$\delta l^* = \arg\min_{\delta l} \| \mathbf{J}\delta l - \delta P \|_2 = \mathbf{J}^\dagger \delta P. \tag{5}$$

The calibration process first calculates the Jacobian, and then applies the Jacobian pseudo-inverse to the difference between measured and simulated PSFs. In practice, S is not linear to l, so we multiply δl by a damping factor $k_d < 1$ [18], and iterate several times until convergence, which typically takes 3 to 5 iterations. The optimization scheme is shown in Fig. 2.

We fit the following parameters in the lens prescription: 1) Radius of curvature, XY offset (perpendicular to the optical axis), and Z offset (parallel to optical axis) of each optical element, 2) Coefficients of the dispersion function formula, and 3) Camera back focal length.

Because we assume spherical lenses, surface tilting can be modeled by a combination of X, Y, and Z offsets. The dispersion function affects chromatic abberation as
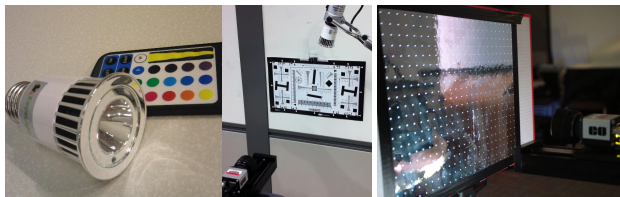
Fig. 5: Experimental Setup. Left: 3-color LED to illuminate resolution charts. Middle: Image collection setup. Right: A precisely constructed pinhole grid pattern. Note: when collecting data, the only light present is due to the LED illuminant.

different wavelengths have different refraction indices. Chromatic abberation is most affected by the first derivative of the dispersion function $\frac{dn}{d\lambda}$, so as a simplification we only optimize this first derivative for each glass.

5   Lens Measurements

The PSF measurement setup is shown in Fig. 5. This consists of an Edmund Optics 5MP monochrome camera. To obtain color images we use a three-color LED illuminant, also shown in Fig. 5.

We found our camera to be relatively noisy due to its small (2.2 μm) pixel size. To correct fixed pattern noise, we captured a textureless white card at two exposure levels and fit a per-pixel offset and gain. Each pixel is corrected to have the same offset and gain. We averaged several images in sequence to reduce the remaining temporally varying noise components.

We tested three different multi-element lenses, shown in Fig. 3, that cover a range of properties that are typically seen in consumer camera lenses. All are off-the-shelf parts purchased from Edmund Optics. We used these lenses because Edmund Optics will provide prescriptions for their lenses, while manufacturers such as Canon will not.

For each image, we measure the object distance and estimate the back focal distance. With these parameters we simulate the point-spread function.

To calibrate and measure our simulated point spread functions we use several precisely constructed calibration targets. To measure effective image resolution, we use a standard I3A/ISO Resolution Test Chart from BHPhoto. To measure impulse responses, we laser-cut $0.1mm$ diameter pinholes into an aluminized Mylar sheet, which was then mounted on a flat acrylic backing coated with a diffusing material. We backlit this target with our LED light source illustrated in Fig. 5.

5.1   Calibration

We calibrated the 3 lenses shown in Fig. 3. The number of variables in 3 lenses are 33, 36, 43 for lenses (a), (b), (c) in Fig. 3, respectively. Non-linear optimization of this number of variables is challenging. The damping factor, k_d, is set to 0.7, and we iterated 5 times.

The calibration process takes 84, 53, and 67 measured PSF samples as input for lens (a), (b), (c), respectively. The numbers depend on the field of view of the lenses. These PSFs are measured at a single focusing distance and captured with a single image. The un-calibrated PSFs has more significant differences at corners, so we sample more densely at the corners than at the center. While we use a single photograph and focal

plane for calibration, the extension to multiple planes is straightforward. The object distances are 279mm, 711mm, 863mm for lenses (a), (b), (c), respectively, to make sure the light sources can cover the whole field of view.

The manufacturing tolerance of each parameter is on the order of 1% [17], so we set the offsets to be 0.5% for radius, $10^{-5}m$ for XYZ offsets, 1% of dispersion at the red frequency [7] for the dispersion function offset, and $10^{-5}m$ for back focal length. The numerical derivatives are approximated with a two sided finite difference.

Both PSF computation and Jacobian calculation can be performed in parallel. Running the calibration on a 4-core machine takes about 6 hours for each lens. Because the simulation and calibration are easily parallelized larger clusters will dramatically reduce this time.

6   Results

In this section, we discuss several experiments used to show that our calibration process is accurate and stable. In lieu of comparing to less accurate parametric models, we have choosen to compare directly to groundtruth measurements, as we felt this was the most rigorous way to show the accuracy of our simulated kernels after calibration. We performed three cross validation experiments to show there is no over-fitting, that we are calibrating accurately, and that the calibration is stable across changes in the lens focus and illuminant spectrum. As appropriate, figures show the corresponding blur kernel sampled from the PSF as an inset image. Please see our supplemental materials for additional results.

Fig. 6 shows the results of image enhancement by deconvolving with simulated PSFs. As was done in the work of Joshi et al. [11], we use Lucy-Richardson deconvolution as this method is less forgiving of errors in blur kernels and thus best conveys the accuracy of the kernel. The results show that compared with the PSF simulated from the lens specification, the PSF from the calibrated lens prescription is closer to the results using the measured PSF. Compared with original images, while the PSF from the un-calibrated lens introduced artifacts when used for deconvolution, our method simultaneously sharpen the image and reduces chromatic aberration with few artifacts just as when using the measured PSF.

In Fig. 7, we show the results after calibrating a lens to get two prescriptions P_a and P_b respectively for two corresponding measured depths D_F and D_S. We then took an image at depth D_S, and deconvolved it with the PSF synthesized at D_S using the prescriptions from both calibration runs, i.e. fitting at the the same depth D_S and a different depth D_F. In all cases and all lenses, regardless of what depth is used for fitting, the deconvolution results significantly reduce chromatic aberrations and sharpen the image. In these experiments, we use a range of depth differences between D_F and D_S − 33% for the #58202, 50% for the #54857, and 8% for the #54854. To the best of our knowledge, no existing parametric model can predict the PSF at different depths, while our method can.

In Fig. 8, we show the result of taking an image at D_S and deconvolving it with the PSF measured at D_F. The result includes noticeable artifacts. The purpose of this

---

[7] in physics, dispersion is defined as $\frac{dn(\lambda)}{d\lambda}$

experiment is to illustrate that the assumption that PSF shape is invariant to focused plane distance is over simplified. One cannot simply measure the PSF at one depth and use it to enhance images from other depths. This shows the importance of our work: one can calibrate the lens prescription at one depth and later simply compute PSFs at different depths to enhance images.

In Fig 12, we show results using more natural images. We also include results for these images of the same cross validation process discussed above. In all cases, our method reduces or removes chromatic aberration and sharpens the images. We compare our method with existing methods in Fig. 10. In Fig.11, we show that our method can easily correct for geometric distortion using the correspondences from ray tracing.

In Fig. 9, we show how our our method can be used to correct images taken under a different illuminant spectrum than was used for calibration. The lens prescription calibrated using measurement under white light spectrum works well on images taken under incandecent fluorescent mixed spectrum. In Fig. 9 we show our method does not even require accurate spectrum information, but we can instead simulate a PSF using standard illuminant spectrum [1] given the white-balance mode of a camera (florescent, tungsten, etc.). The approximate fluorescent mixed spectrum [1] and white light spectrum (Figs. 9 (c)(d).) generate comparable results to using actual measure spectrum information (Fig. 9 (b).)

7   Conclusions

Our method improves image quality by deblurring images using point-spread functions computed with wave optics and a calibrated lens model. These point-spread functions model all optical aberrations. Previous work has addressed these optical artifacts as separate problems, while our approach unifies all of these corrections into one process.

Our method requires roughly two orders of magnitude fewer calibration images than strictly measurement based methods. Our fitted lens model generalizes to conditions far outside of those captured during calibration. After calibration the PSF can easily be simulated at any desired focus distance, lens aperture, or image plane position. We have demonstrated that the match between our fitted model and a measured PSF is very good, even when the lens calibration and PSF simulation are done at different depths.

Unlike previous methods, ours generalizes to illumination spectra different from that used to capture the calibration image. Ideally the precise illumination spectrum would be known but one can still improve images significantly if the lighting spectrum is unknown.

References

1. http://www.cis.rit.edu/research/mcsl2/online/cie/fluorescents.htm.

2. M. R. Banham and A. K. Katsaggelos. Digital image restoration. *Signal Processing Magazine, IEEE*, 14(2):24–41, 1997.

3. J. Brauers, C. Seiler, and T. Aach. Direct psf estimation using a random noise target. In *Digital Photography*, page 75370, 2010.

4. M. Cannon. Blind deconvolution of spatially invariant image blurs with phase. *Acoustics, Speech, and Signal Processing [see also IEEE Transactions on Signal Processing], IEEE Transactions on*, 24(1):58–63, 1976.

5. W. T. Cathey and E. R. Dowski. New paradigm for imaging systems. *Appl. Opt.*, 41(29):6080–6092, Oct 2002.

6. J.-A. Conchello and J. W. Lichtman. Optical sectioning microscopy. *Nature Methods*, 2(12):920–931, Nov. 2005.

7. R. Fergus, B. Singh, A. Hertzmann, S. T. Roweis, and W. T. Freeman. Removing camera shake from a single photograph. *ACM Trans. Graph.*, 25:787–794, July 2006.

8. J. W. Goodman. *Introduction to Fourier Optics*. 2005.

9. P. Hanrahan and R. Ng. Digital correction of lens aberrations in light field photography. In *International Optical Design*, page WB2. Optical Society of America, 2006.

10. G. Hausler. A method to increase the depth of focus by two step image processing. *Optics Communications*, 6:38–42, 1972.

11. N. Joshi, R. Szeliski, and D. J. Kriegman. Psf estimation using sharp edge prediction. In *Computer Vision and Pattern Recognition, 2008. CVPR 2008. IEEE Conference on*, pages 1–8, 2008.

12. S. Kang. Automatic removal of chromatic aberration from a single image. In *Computer Vision and Pattern Recognition, 2007. CVPR'07. IEEE Conference on*, pages 1–8. IEEE, 2007.

13. E. Kee, S. Paris, S. Chen, and J. Wang. Modeling and removing spatially-varying optical blur. In *Computational Photography (ICCP), 2011 IEEE International Conference on*, pages 1–8. IEEE.

14. J. E. Krist. Deconvolution of hubble space telescope images using simulated point spread functions. *Astronomical Data Analysis Software and Systems*, 1992.

15. A. Levin. Blind motion deblurring using image statistics. In *NIPS*, pages 841–848, 2006.

16. A. Levin, P. Sand, T. S. Cho, F. Durand, and W. T. Freeman. Motion-invariant photography. *ACM Trans. Graph.*, 27:71:1–71:9, August 2008.

17. J. McGuire Jr et al. Designing easily manufactured lenses using a global method. In *International Optical Design Conference*. Optical Society of America, 2006.

18. J. Meiron. Damped least-squares method for automatic lens design. *JOSA*, 55(9):1105–1107, 1965.

19. S. K. Nayar, M. Watanabe, and M. Noguchi. Real-time focus range sensor. *IEEE Trans. Pattern Anal. Mach. Intell.*, 18:1186–1198, December 1996.

20. B. Scalettar, J. Swedlow, J. Sedat, and D. Agard. Dispersion, aberration and deconvolution in multi-wavelength fluorescence images. *Journal of microscopy*, 182(1):50–60, 1996.

21. L. Xu and J. Jia. Two-phase kernel estimation for robust motion deblurring. In *Proceedings of the 11th European conference on Computer vision: Part I*, ECCV'10, pages 157–170, Berlin, Heidelberg, 2010. Springer-Verlag.

22. C. Zhou, S. Lin, and S. Nayar. Coded aperture pairs for depth from defocus. In *ICCV*, Kyoto, Japan, Oct 2009.
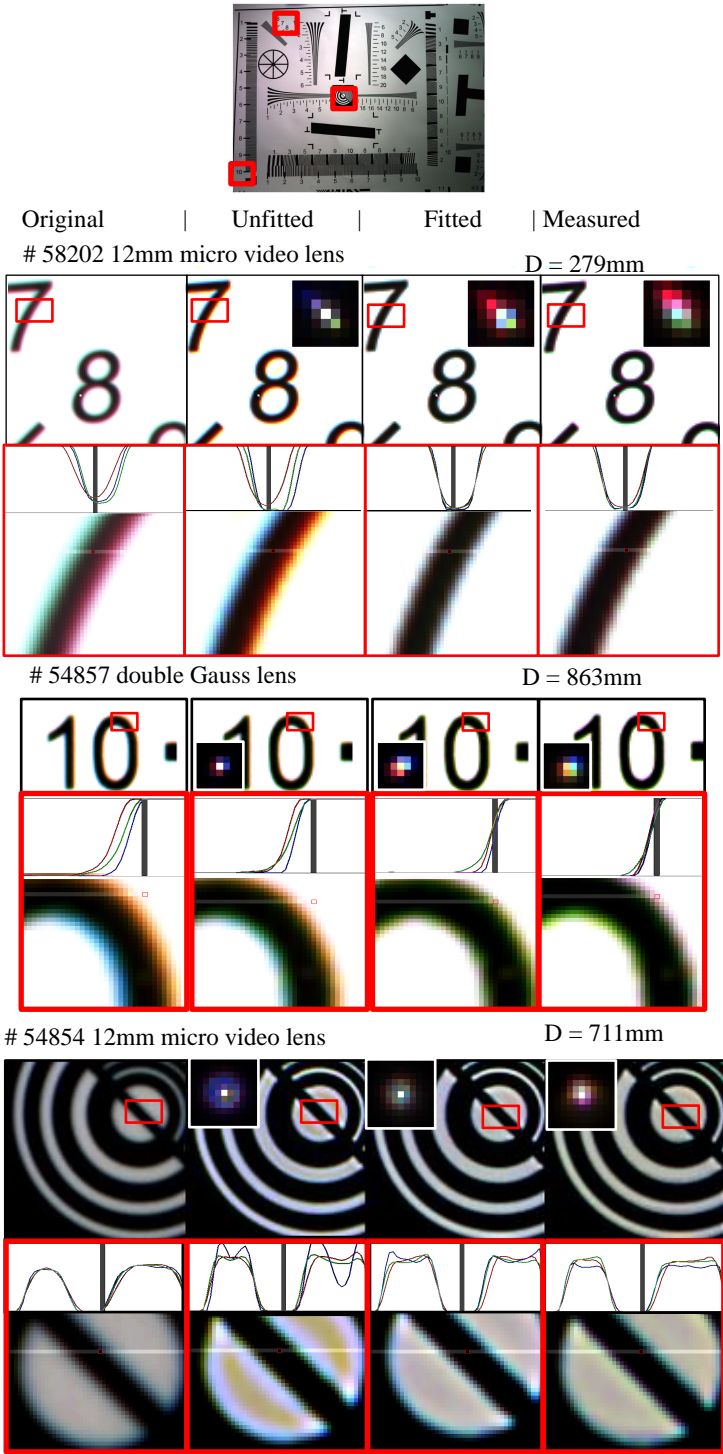
Fig. 6: Cross validation across the image plane. Original images taken at D (first col.), images deconvolved with PSFs simulated using nominal (un-calibrated) and calibrated lens prescription (second and third col.), and with measured PSFs (fourth col.). The 1-D horizontal slice of insets shows the calibrated version sharpens the image and reduces the chromatic aberration in all lenses.
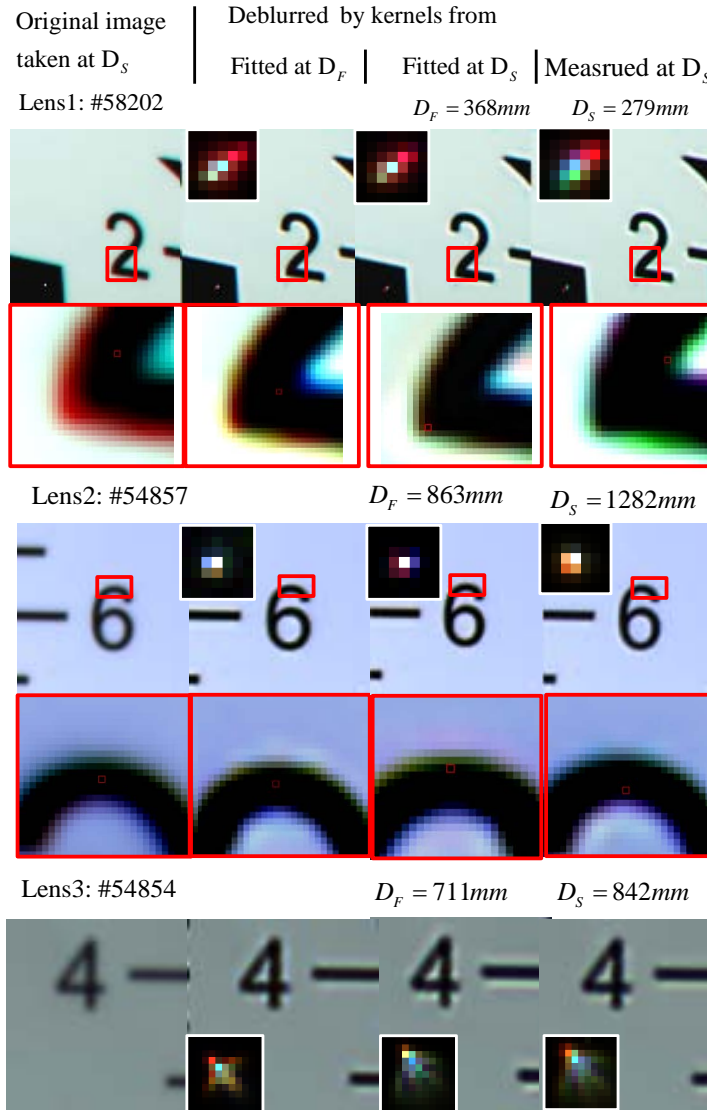
Fig. 7: We calibrated at two different depths D_F and D_S, respectively, then took an image at depth D_S, and deconvolved it using PSFs synthesize at D_S. Original images (first col.), images deconvolved using the PSFs from each calibration (second and third col.), and images deconvolved by PSF measured at D_S, i.e., the "groundtruth" (fourth col.). The image enhancement is equally good regardless of which depth is used for fitting.

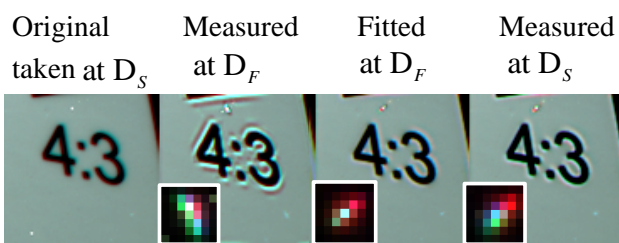| Original | Measured | Fitted | Measured |
| taken at D_S | at D_F | at D_F | at D_S |

Fig. 8: For an image at $D_S = 368mm$ (first col.), we deconvolve with a PSF measured at $D_F = 279mm$ (second col.), a PSF computed by calibration at D_F (third col.), and a PSF measured at D_S, i.e. "groundtruth" (fourth col.). Measurements do not generalize across different depths, while our method does.

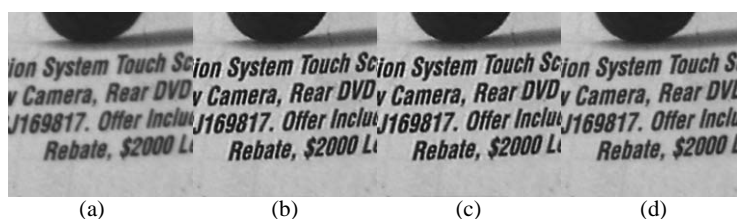(a)   (b)   (c)   (d)

Fig. 9: Validation under different lighting conditions. Original image taken under incandecent/fluorescent mixed spectrum (a), deblurred by PSF fitted under white light (RGB LED)(b), deblurred results using PSF computed by approximate tungsten/fluorescent spectrum (c) and white light spectrum (d), instead of measured spectrum in (b). Our method gives good results even if the eaxt spectrum is not known.

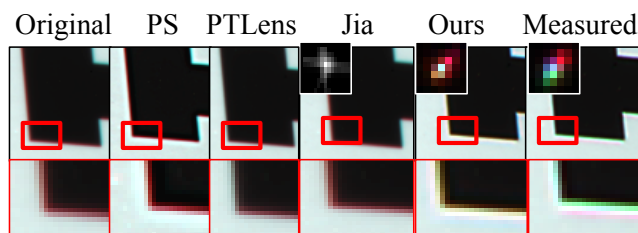Original   PS   PTLens   Jia   Ours   Measured

Fig. 10: Comparison with Photoshop smart sharpening (lens blur mode), PTLens chromatic aberration removal, Jia et al.'s robust motion deblurring.
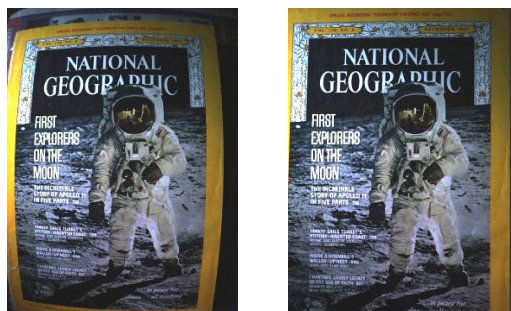

Fig. 11: Geometric distortion can be easily corrected for using our method.

Fig. 12: Image enhancement results of a newspaper and a National Geographic magazine cover. We take a image (first col.), and fit lens prescriptions at two different depths, respectively, and use them to enhance the image (second and third col.). The insets show reduced abberations and chromatic aberrations.